Epitaxial Growth of III-Vs on On-Axis Si: Breaking the Symmetry for Antiphase Domains Control and Burying

Audrey Gilbert, Michel Ramonda, Laurent Cerutti, Charles Cornet, Gilles Patriarche, Éric Tournié, Jean-baptiste Rodriguez

ADVANCED OPTICAL MATERIALS
www.advopticalmat.de

Epitaxial Growth of III-Vs on On-Axis Si: Breaking the Symmetry for Antiphase Domains Control and Burying

*Audrey Gilbert, Michel Ramonda, Laurent Cerutti, Charles Cornet, Gilles Patriarche, Éric Tournié, and Jean-baptiste Rodriguez**

Abstract: This work reports on the precise control of III-V semiconductors' antiphase domain formation and evolution during the epitaxial growth on an "on-axis" Si (001) substrate with a very low but controlled miscut. Especially, it is shown how, starting from a Si surface having a regular array of terraces, the crystal polarity of thin GaAs epilayers grown by molecular-beam epitaxy is defined through the Si surface topology, leading to a quasi-periodic 1D pattern of antiphase domains in the GaAs layer. Furthermore, this work demonstrates how this configuration breaks the symmetry between the two different III-V phases, without any step-flow-induced asymmetry. Following this strategy, an early burying of antiphase domains is demonstrated in GaAs epitaxially grown on a low-miscut Si substrate. This study generalizes previous models describing antiphase domain formation and evolution and establishes the important growth parameters for the development of high crystal quality III-V semiconductor devices monolithically integrated on low-miscut silicon substrates.

1. Introduction

Due to its abundance, optical transparency windows, and high refractive index, Si is the most widely used material for integrated photonics at datacom and telecom wavelengths.[1] However, although Si can efficiently transmit, modulate, and detect light, its indirect band gap forbids light emission.[2] As a result, the integration of III-V lasers on Si platforms has for long attracted much interest to develop photonic integrated circuits (PICs) for high-speed optical communications and chemical or biological sensors.[3] Indeed, the co-integration of PICs on industry-standard platforms promises high performance, new functionality, ultralow cost, large integration density, and scalability.

Despite the many bonding techniques developed over the years,[4] monolithic integration has emerged as a promising solution to integrate optical emitters directly onto a Si platform with low-cost and high density.[5] However, epitaxially integrated devices suffer from a severe lack of reliability because of the large crystal-defect density created during growth. In particular, antiphase boundaries (APBs), the first and most problematic defect, are induced by the heteroepitaxy of polar III-Vs on nonpolar Si substrates. Silicon diamond structure contains only one type of element unlike the III-Vs, which allows the formation of two polar domains (antiphase domains, APDs) delimited by APBs. These boundaries form electrically charged paths inside the materials and create shortcuts that kill devices. Thus, they must be avoided, or at least they should be confined below the active part of the device.

This problem was initially studied by Kroemer for the growth of GaAs on Si[6] who proposed that APDs, and thus APBs, can be avoided by promoting the formation of bi-atomic steps at the Si surface. Highly misoriented substrates create double steps, which promote the growth of the same polar variant in the entire crystal.[6–8] However, Akiyama et al. and Pukite et al. later demonstrated that double steps are not necessary to obtain GaAs layers free of emerging APBs.[9,10] The growth of a single domain on (001) Si was attributed to APBs self-annihilation, but no clear explanation of the mechanism was provided.[9,10] Furthermore, Georgakilas et al. suggested that APDs annihilation results from a tilt of the APBs toward the (001) plane.[11] Also, their observations indicated that the nucleation temperature determines the domains' density and size. At low nucleation temperatures, the coalescence of small domains promotes APDs self-annihilation faster than large domains grown at high temperatures. Altogether, and in spite of recent demonstrations of APBs-free GaAs

A. Gilbert, L. Cerutti, É. Tournié, J.-baptiste Rodriguez
IES
University of Montpellier
CNRS, Montpellier F- 34000, France
E-mail: jean-baptiste.rodriguez@umontpellier.fr
M. Ramonda
CTM
University of Montpellier
Montpellier F- 34000, France
C. Cornet
Univ Rennes
INSA Rennes
CNRS, Institut FOTON, UMR 6082, Rennes F-35000, France
G. Patriarche
C2N
University of Paris Saclay
CNRS, UMR, Paris 9001, France

The ORCID identification number(s) for the author(s) of this article can be found under https://doi.org/10.1002/adom.202203050

DOI: 10.1002/adom.202203050

layers on on-axis (001) Si substrate[12,13] the physical insights into the phenomenon remain unclear. The purpose of this article is to solve this long-standing issue.

2. Symmetry Breaking Resulting from a "Terrace-Driven" Initial Phase Distribution

Recently, a new theoretical perspective for forming and burying APDs on low-miscut Si substrates was proposed.[14] This theory is based on the observation that most III-V semiconductors cannot wet the Si substrate, which results in the formation of individual monophase 3D Volmer–Weber islands.[15] Especially, it was demonstrated that these islands can grow and reach sizes significantly larger than distances between monoatomic steps at the Si surface.[15] The fact that a single monophase III-V island can be formed over one or several Si monoatomic steps demonstrates that the chemistry of the III-V/Si interface, and more specifically the charge compensation in the intermixed III-V-Si atomic layers[16] is not homogeneous within one large monophase islands. It also shows that, during the growth of an individual island over a monoatomic step, the rearrangement of the III-V/Si interface is energetically preferred over the formation of an antiphase boundary.

The proposed antiphase burying model assumes that the phase (or polarity) of the nucleated individual islands is governed by the orientation of the dimers on the Si terraces on which the nucleation initially occurs.[14] From this hypothesis, it was deduced that the initial domain distribution can be inferred from the comparison between the stable III-V islands' typical size, and the Si terrace width. Two regimes were identified:

First, when the III-V islands are smaller than the terrace width, the local Si dimer orientation imposes the same phase for the numerous III-V islands nucleating on the same terrace, and the phase distribution after islands coalescence is therefore "terrace-driven." If the Si surface is populated by monoatomic height steps, the terraces form parallel stripes of alternating dimer orientations. As the III-V growth is initiated, the initial phase distribution mimics this organization and forms stripes of alternating phases. The width of the stripes corresponds in first approximation to the Si terrace width and is therefore strongly related to the miscut value when the substrate surface is properly prepared.[12]

On the contrary, if the stable islands have a larger size than the terrace width, the phase of individual islands is also governed by the local dimer orientation, but the monophase islands grow over several Si steps before they can coalesce. The APD distribution is then "nucleation-driven," and the initial phase distribution no longer reproduces the Si terraces topology, but rather reflects the islands' nucleation density.

Of course, in the case of a double-stepped Si starting surface (as obtained by preparation in metal-organic chemical vapor deposition conditions[17–19] or sometimes with the use of large miscut substrates[8]), the adjacent terraces have the same dimer orientation, which results in a monophase III-V layer once all the islands have coalesced. Still, it is extremely difficult to achieve a perfectly double-stepped Si surface, which results in residual APDs.[17]

In the case of a single-stepped Si starting surface, the previously developed model[14] describes the burying of one of the two domains (the so-called APD) by the other (the main-phase domain—MPD) because the two domains have steps of different kinds (V or III steps), which translate in a growth rate difference related to the preferential incorporation of the element-III on one of the two kinds of steps, depending on the growth conditions. The fastest-growing domain overgrows the other one at some point. Again, the substrate miscut is of prime importance as it allows for generating a surface where the III-steps are predominant in one of the two domains, while the other is mostly populated by V-steps, which is the key factor triggering the growth rate imbalance. In that case, the burying is due to the different atomic compositions of the steps found in each domain. In fact, the higher symmetry of the Si Diamond crystal with respect to the III-V zinc-blende crystal—leading to the formation of the APDs in the first place—is broken by the unidirectionality of the steps at the growth front over the whole sample. The two [110] main crystallographic directions are equivalent in Si, which allows the growth of the two III-V phases at its surface, but the unidirectionality of the steps creates an anisotropy (which translates into the different atomic composition of the steps and thus in anisotropic incorporation rates) leading to the selection of one of the two phases. The proposed mechanism is therefore strongly related to the step-flow growth mode, which is required to maintain the steps distribution and unidirectionality as the growth proceeds. This burying mechanism was later experimentally confirmed and extensively studied for the growth of GaSb on low-miscut (001) Si.[20] The necessity of having the same Si step direction on the whole substrate surface, which can only be obtained when the miscut direction points toward one [110] direction of the Si substrate, and of maintaining a step-flow growth mode of the III-V was also demonstrated. In particular, no burying could be observed at low temperatures, where the step-flow is hindered. This study was an important experimental demonstration of the burying mechanism, which allows explaining the annihilation of APBs through the differences that can exist between the growth kinetics of the two phases, rather than from the APBs propagating in different crystallographic planes. Still, at this stage, the nature of the initial phase distribution and its influence on the APDs burying was unclear and had not been studied experimentally, which is missing to have a complete demonstration of the mechanism at play. Moreover, the influence of high index surface facets that are formed at the vicinity of emerging APBs[21] on the burying process of APDs was not properly discussed yet in the framework of this APD burying model.

The present paper aims at clarifying the role of the initial phase distribution by studying the growth of GaAs on low miscut (001) Si substrates. GaAs is indeed an interesting III-V material as it generates small stable islands (about a factor of ten smaller compared to GaSb for instance). The stable island size indeed depends on the material (as well as on the growth conditions of course), and therefore so does the maximum miscut angle at which the transition from the "terrace-driven" to the "nucleation-driven" regime can be observed. Interestingly, the expected stable island size for GaAs in standard conditions (a few tens of nanometers) allows reaching such a transition at reasonable substrate miscut values (0.2° to 0.5°) by changing the growth temperature.[14] Besides, the epitaxy of GaAs on Si is of technological importance for the realization of photonic integrated circuits such as optical interconnects.

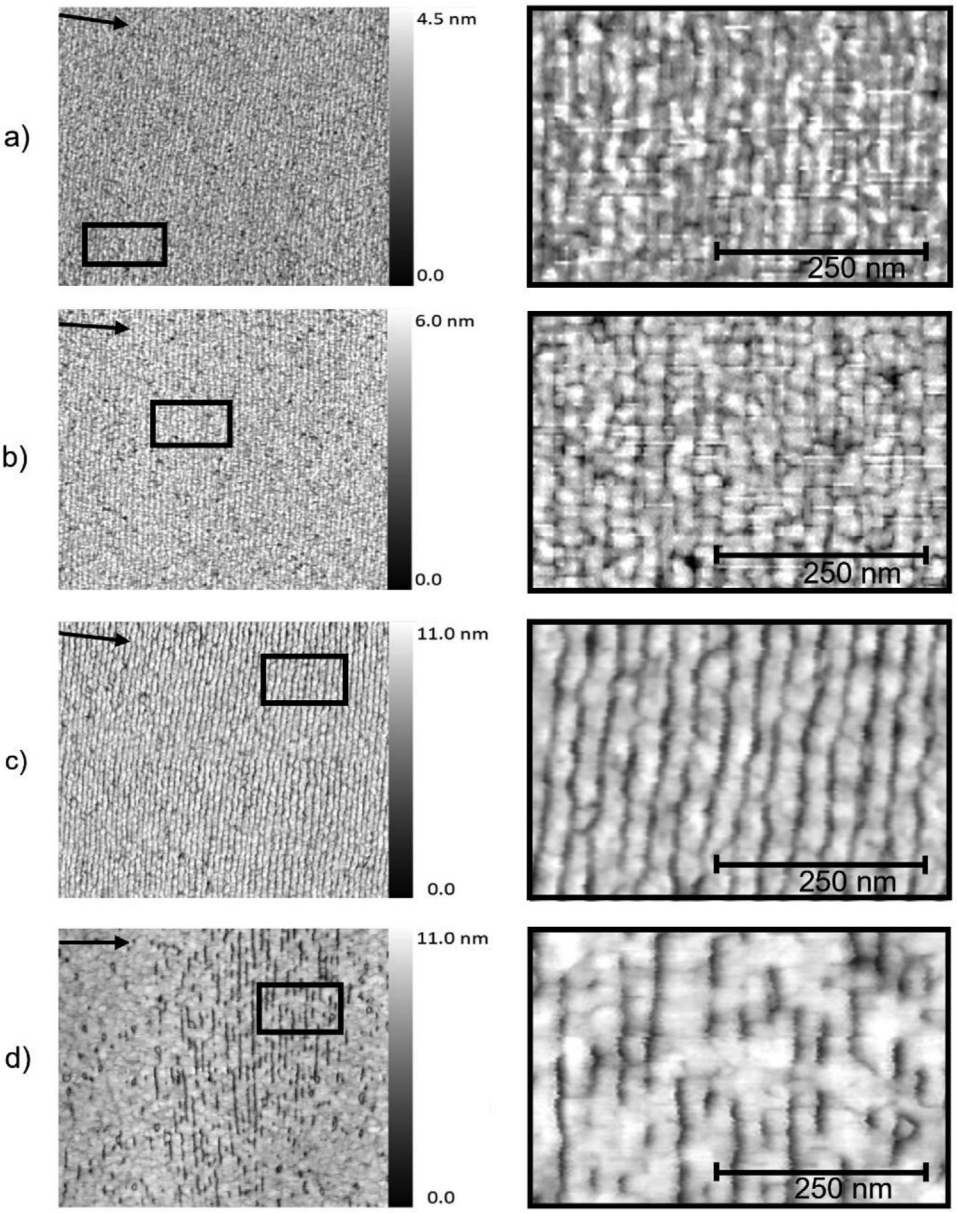

Figure 1. A 2 × 2 μm^2 atomic force microscopy (AFM) images of a) 25 nm, b) 50 nm, c) 100 nm, d) 110 nm GaAs layers grown on (001) Si. The areas shown in the rectangles are displayed with a higher magnification on the right of each image. The period and the narrowing of the darker stripes with the increasing thickness are presented, and the black arrows indicate the miscut direction.

3. Results and Discussion

3.1. Identification of the Initial Phase Distribution

In this section, we study GaAs layers grown on (001) Si to evidence the initial phase distribution by comparing atomic force microscopy (AFM) and cross-sectional transmission electron microscopy (TEM) data. We demonstrate that, in our growth conditions and with our substrate preparation, GaAs is grown in the "terrace-driven" regime and that increasing the nominal GaAs thickness leads to the progressive burying of one of the two phases. This mechanism proves to be very effective and can be used to obtain emerging-APB-free GaAs layers for thicknesses as low as 150 nm with low-miscut substrates.

The GaAs layers were grown on low-miscut Si substrates by molecular-beam epitaxy (MBE). Note that the substrates were randomly chosen within a batch ordered with a specified miscut angle and direction, which can easily be obtained through most of the wafer suppliers. Care was taken to repeat several times some experiments to ensure that the whole substrate preparation as well as the entire growth procedure (which is described in more detail in the Experimental Section at the end of this paper) is reproducible. **Figure 1** shows AFM images of 25, 50, 100, and 110 nm thick GaAs layers grown on (001) Si substrates with

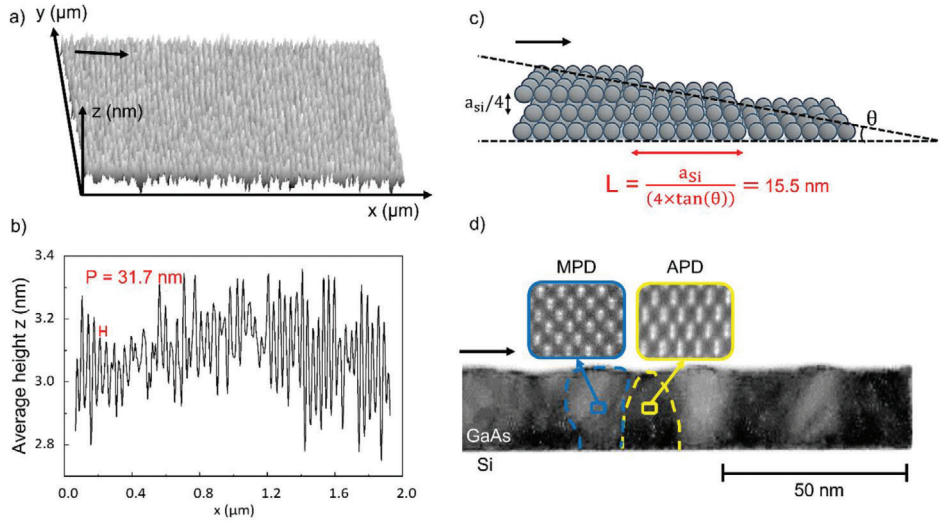

Figure 2. a) A 2 × 2 μm^2 atomic force microscopy (AFM) image of 25 nm GaAs layer and b) average height of the pattern. c) Evolution of the terraces' width (L) for Si monoatomic steps with the miscut angle θ. d) Bright field scanning transmission electron microscopy (STEM) cross-section of the interface Si-GaAs showing the initial periodic islands repetition and HAAADF–STEM insert of V-polar main domain consisting in arsenic atom (brighter) upward, while III-polar antiphase domain (APD) has arsenic atom downward. Black arrows indicate the miscut direction

an offcut of 0.5° toward [110]. A succession of elongated dark and bright parallel stripes is seen at the surface of the thinnest sample (Figure 1a). As the thickness increases, the depth difference between dark and bright stripes increases which leads to a larger roughness, while the width of the darkest stripes shrinks (Figure 1b,c). At a nominal thickness of 110 nm (Figure 1d), most of the dark stripes have been overlaid by the bright ones. Even at larger image scales, all samples show such homogeneous surface features.

A striking feature observed on all samples is the succession of these straight dark and bright stripes in a quasi-perfect periodic network. We measured this periodicity on the sample having the thinnest GaAs layer with the Gwyddion software. To this end, the x and y axis of the images were first carefully aligned along the [110] main crystallographic directions of the silicon substrate. Then, the average height z in the y direction was calculated and plotted for each x position in **Figure 2**b. The resulting curve shows periodic oscillations, and the period corresponds to the sum of the widths of one dark and one bright stripe. The value retrieved from this statistical analysis (31.7 ± 0.3 nm) is very close to the calculated width of two terraces at the Silicon surface for a miscut of 0.5° (31.0 nm, see Figure 2c). From there, we conclude that the periodic topography observed at the surface of these samples is strongly related to a homogeneous distribution of monoatomic steps lying along the [110] direction at the Si surface prior to the growth. It is worth emphasizing that such a distribution can only be obtained when the miscut direction points toward one [110] direction of the Si substrate.

In order to clarify the structural difference between the dark and bright stripes, a TEM analysis was carried out on the same sample. Figure 2d presents a cross-sectional TEM image taken in the direction perpendicular to the stripes observed at the sample surface. These measurements allow identifying the periodical features seen by AFM. More importantly, it confirms that this alternating bright-and-dark-stripes configuration results from the periodical arrangement of the MPDs and APDs in these GaAs layers. Indeed, the inset of Figure 2d shows the dumbbell orientation in the two regions. The inversion of arsenic and gallium atoms' position unambiguously indicates the presence of two crystal phases highlighted in yellow and blue. Combined with the larger-scale analysis of the AFM data presented above, this crucial observation demonstrates that the APD–MPD arrangement at this stage is directly correlated with the step distribution at the Si surface prior to the growth, or in other words, that the initial phase distribution growth is "terrace-driven." Such results are compatible with Li et al.'s recent work[12] reporting that the Si substrate played a significant role in APBs annihilation in GaAs and showed a clear correlation between the III-V domain phases and Si terraces.

3.2. Initial Phase Distribution Temperature Dependence

The burying model described above is based on the hypothesis that the initial phase distribution depends on the relative size of the stable III-V island, with respect to the Si terrace width. The distribution is "terrace-driven" if the stable III-V island size is small compared to the terrace width, and "nucleation-driven" otherwise. In the latter case, the initial phase distribution is not anymore correlated to the Si terraces arrangement and is therefore randomly organized. In an attempt to assess the validity of this assumption, we decided to study the impact of the substrate temperature on the phase distribution. It is well known that the size of stable III-V islands increases with the growth temperature, while their density decreases.[22] We therefore aimed at verifying whether increasing the size of the stable island by modifying the substrate temperature allowed transitioning from the "terrace-driven" to the "nucleation-driven" distribution. **Figure 3** displays the AFM images of 50 nm thick GaAs layers grown on Si substrates with a 0.5° miscut at temperatures in the 350 °C to 520 °C range.

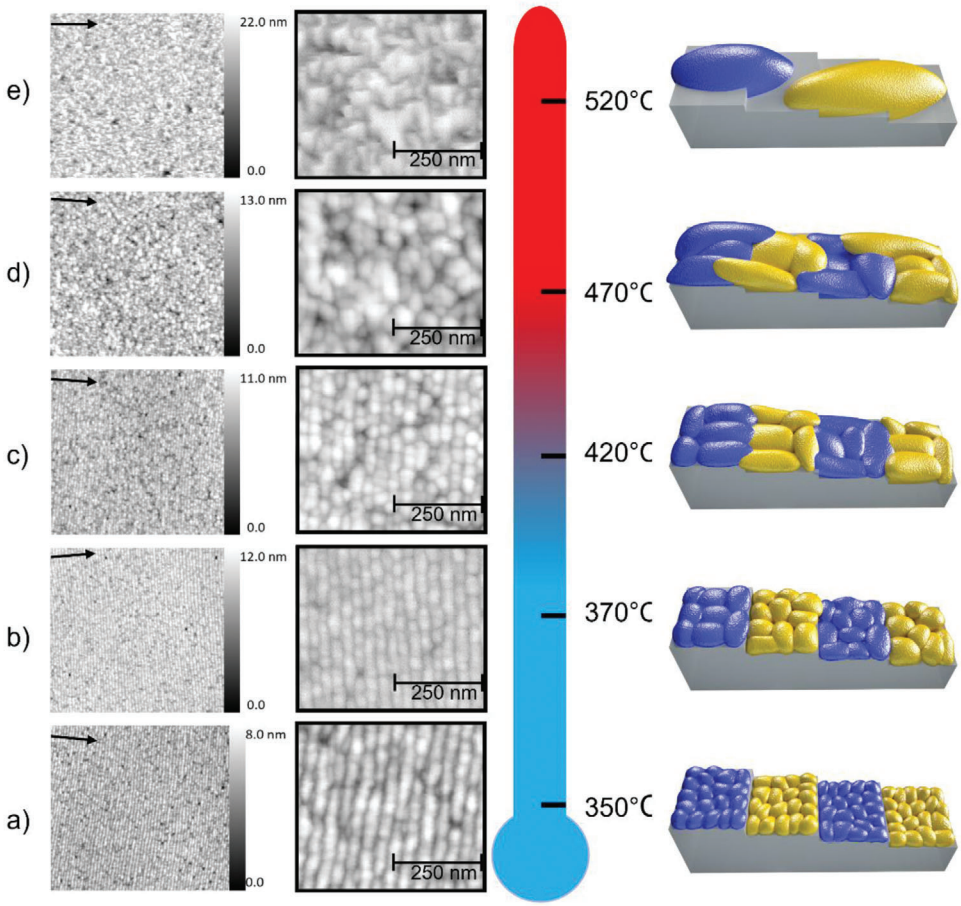

Figure 3. A 2 × 2 μm^2 atomic force microscopy (AFM) images of the surface evolution and zoom of the striped pattern for a) 350 °C, b) 370 °C, c) 420 °C, d) 470 °C, and e) 520 °C for 50 nm samples and stable island size in the initial phase distribution at low thickness. Black arrows indicate the miscut direction.

At the lowest temperatures, the alternating MPD/APD stripes are clearly visible, which confirm the "terrace-driven" nature of the initial phase distribution described above (Figure 3a,b). As the temperature is increased to 420 °C and then 470 °C (Figure 3c,d), the stripes arrangement degrades, and finally, the surface morphology of the sample grown at 520 °C is completely randomly shaped (Figure 3e). As expected, the high-growth temperatures lead to bigger initial islands, which is confirmed by the increase of the surface roughness as well as by the loss of the phase organization. The results obtained from this set of samples are therefore clearly compatible with the transition from one regime to the other at a temperature between 420 °C and 470 °C. It can also be concluded that in our growth conditions and in this transition temperature range, the average size of the nucleated stable islands just before coalescence is expected to lie around 15.5 nm, the Silicon terrace width prior to growth.

3.3. APD Burying in the "Terrace-Driven" Regime

The evolution of the APD dark stripes morphology with the GaAs nominal thickness observed earlier (Figure 1a–d) provides some valuable information on the overgrowth mechanism itself. First of all, the MPD grows faster in the growth direction as attested by the increase of the average height difference between the MPD and APD. We roughly estimated this growth rate difference by calculating the mean height of both domains on the AFM data shown in Figure 1. The MPD grows about 2.7% faster than the APD, which is comparable to the value of 3.2% found in the case of GaSb grown on Si.[20] Additionally, as the thickness of GaAs increases, the width of the dark stripes shrinks, indicating that the MPD not only grows in height but also laterally at a faster rate. This results in the coverage of the APD by the MPD stripes, eventually leading to their burial. This indicates that the burying mechanism by which the MPD overgrowth the APD is already active, even for a GaAs thickness as small as 25 nm.

To demonstrate the complete APD burying, a sample with a 500 nm thick GaAs layer was grown and characterized by AFM and cross-sectional scanning transmission electron microscopy (STEM) (**Figure 4**a,b). The surface of the sample shows a roughness as low as 1.38 nm and elongated topographical features parallel to the miscut (Figure 4a). The STEM data show that the APDs are completely buried within about 150 nm (Figure 4b), which is consistent with the observation previously made that APDs start to disappear from the surface after around 110 nm of GaAs (Figure 1d).

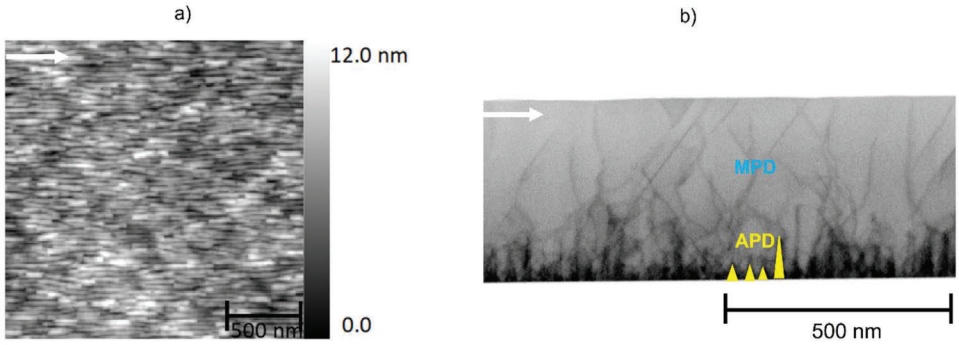

Figure 4. a) A $2 \times 2\ \mu m^2$ atomic force microscopy (AFM) image and b) bright field scanning transmission electron microscopy (STEM) images of 500 nm GaAs antiphase boundaries (APBs) emerging free layer grown on 0.5° Si (001) substrate. White arrows indicate the miscut direction.

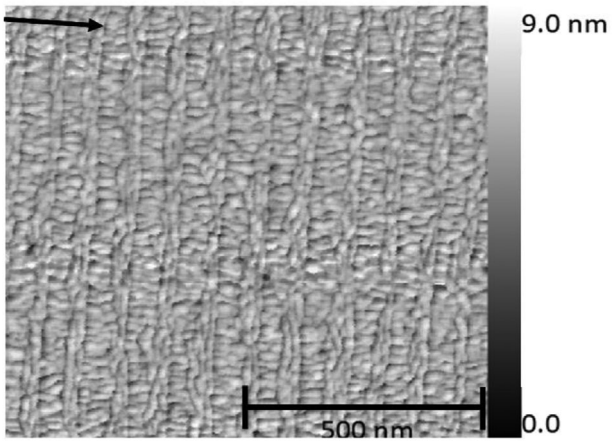

Figure 5. A $1 \times 1\ \mu m^2$ atomic force microscopy (AFM) image of the 50 nm GaAs layer grown on 0.2° Si substrate, the black arrow indicates the miscut direction.

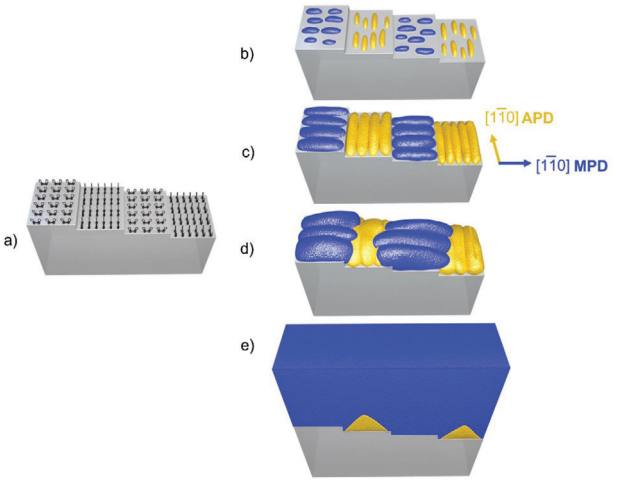

Figure 6. a) Monoatomic stepped Si (001) surface with alternating dimers orientation terraces, b) first 3D islands confined on Si terraces, c) growth and nucleation of polar monodomains, d) early overgrowth of the MPD, and e) the antiphase domain (APD) is buried. [1$\bar{1}$0] directions for both APD and MPD are indicated.

Furthermore, we grew a 50 nm thick GaAs layer on a (001) Si substrate with a 0.2° offcut toward [110] to complement our study. **Figure 5** displays a $1 \times 1\ \mu m^2$ AFM image of the sample surface. Similarly to what was observed in the case of a 0.5° miscut, the two phases are clearly visible and arranged in a periodic pattern along one of the two [110] crystallographic directions of the Si substrate. The average periodicity of the APD/MPD pattern extracted from the AFM data equals 82 nm. A value that once again precisely corresponds to twice the calculated terrace size for a 0.2° miscut substrate, and further demonstrates the "terrace-driven" nature of the initial phase distribution in our growth and substrate preparation conditions.

Finally, the AFM image of Figure 5 provides a decisive insight into the way the MPD overgrows the APD at low temperature. One can notice the elongated shape of the islands, which is a well-known feature in the 3D growth of III-V semiconductors.[23,24] Combined with the previous observation, the mechanism can thus be summarized as follows:

I. First, after careful deoxidation, the Si substrate is homogeneously populated by monoatomic height steps having the same [110] direction and a fixed width imposed by the miscut angle value and direction. Two successive terraces have different dimer orientations, which stem from the monatomic height step existing in between (**Figure 6**a).
II. After the epitaxial growth of a few nanometers of GaAs, 3D monodomain stable islands of a smaller size than the terrace width are formed. The phase of each island is thus determined by the Si surface-dimer orientation prior to growth (Figure 6b). Islands of the same phase grow and coalesce on a given terrace, but two adjacent terraces are populated with islands of opposite phases. At some point, each phase covers one in two terraces (Figure 6c). As a result, the domains are arranged in a periodic APD/MPD sequence mimicking the initial terraces dimers distribution, which indicates that the initial III-V phase distribution is "terrace-driven" according to the burying model.[14]
III. Due to the anisotropy of the diffusion length of Group-III atoms, the islands elongate in the [1$\bar{1}$0] direction, as demonstrated by Ohta et al.[25] (the diffusion coefficient is larger in the [1$\bar{1}$0] azimuth, the direction in which islands therefore grow faster). However, the [1$\bar{1}$0] direction in the APD is perpendicular to the [1$\bar{1}$0] direction in the MPD due to

the very nature of the two domains type (see the crystal orientations schematics in Figure 6c). As a result, the islands within the MPD grow faster in the direction pointing toward the APD stripe, and eventually, the MPD overflows the adjacent steps to overgrow the APDs stripes (Figure 6d). By contrast, in the APD, the island's fast-growing direction favors the growth within the APD stripe itself. The expansion of this phase over the MPD is therefore much slower. In other words, the direction along which the islands elongate is different in the two phases, and one progressively extends over the other and becomes the MPD. As the growth proceeds, the APD stripe width gradually decreases until it is buried within about 150 nm in the work presented here for a 0.5° miscut. Note that the miscut value and direction along one of the [110] direction of the Si substrate plays a crucial role here as it allows for forming unidirectional and uniform stripes of the two domains after the III-V islands have coalesced.

IV. Finally, when enough material is deposited (at 500 nm for example in our experiment), the GaAs layer exhibits a flat surface (Figure 6e) free of emerging APBs.

As predicted by the burying model, the additional symmetry of the diamond structure compared to the zinc-blende is reduced in both "terrace-driven" and "nucleation-driven" regimes:

In our previous work,[20] the different incorporation rates at the III- and the V- steps in a step-flow growth mode constituted the growth-related anisotropy that favored one of the two phases.

However, in the present work, the asymmetry is provided by the "terrace-driven" nucleation of the two phases, and is combined with the anisotropic growth of the 3D III-V islands. The symmetry is broken by the formation of a regular array of Si terraces/steps along a given [110] direction through the precise transfer of the miscut. Of importance, this mechanism happens at a very early stage of the growth and does not require that a specific growth mode be maintained to be effective, which certainly makes it more robust to the presence of other topographic features such as the high-index facets commonly observed during the growth of GaAs/Si or GaP/Si,[15,21] while the step-flow required in the other symmetry-breaking mechanism, can be deeply hindered by these facets.

4. Conclusion

In this study, we have demonstrated that modifying the GaAs stable island size, by changing the growth temperature, allows switching from a "terrace-driven" initial phase distribution at low temperatures (where the stable islands are smaller than the Si terrace width), to a "nucleation-driven" initial phase distribution at high temperature (where islands are larger than the Si terrace width). We also demonstrated that, in the "terrace-driven" regime, when the domains are organized in regular stripes of alternating phases, one domain overgrows the other despite the low substrate temperature preventing any symmetry-breaking mechanism based on the combination of the unidirectional steps' initial distribution and step-flow growth mode discussed in our previous report.[20] Finally, a careful study of GaAs layers grown on very small miscut substrates (0.2°) allowed us to unravel the burying mechanism at work in this configuration. Besides, we demonstrated APB-free GaAs surfaces for a layer with nominal thickness as low as 150 nm for a substrate miscut of 0.5°.

In good agreement with the model developed by Cornet et al.,[14] we found that a burying process is responsible for the APD overgrowth. The homogeneous transfer of the miscut was found to be crucial, as it allows for reducing the high symmetry of the Diamond Si crystal. This creates a specific arrangement of the Si terraces which is then combined with a "terrace-driven" initial phase distribution thanks to the low-temperature nucleation of the III-V islands to form straight stripes of alternating phases. We then showed how the anisotropic growth of the III-V islands resulting from the different diffusion lengths of the group III atom in the $[1\bar{1}0]$ and [110] directions is responsible for the burying of one of the two phases, as the MPDs tend to grow faster in the direction of the APD stripes, progressively reducing the latter width until they are completely buried. These findings allow for a global understanding of the combined symmetry-breaking of the group IV crystal and III-V growth asymmetry processes required to efficiently bury APDs, and provide a clear path toward the realization of high-performance III-V devices monolithically integrated on Si platforms.

5. Experimental Section

All the samples were grown by solid-source molecular beam epitaxy in a RIBER COMPACT 21 system equipped with a valved cracker cell for Arsenic. Small offcut angle (001) Si substrates were used for this study, and the surface was thermally prepared in situ (above 1 000 °C), in a dedicated chamber, to remove the native oxide. The procedure was carefully applied for all the samples of this study, ensuring a good reproducibility of the observations. In these conditions, the reflection high-energy electron diffraction reflection high-energy electron diffraction (RHEED) pattern of the Si surface shows a superposition of (1 × 2) and (2 × 1) reconstructions, indicating the formation monoatomic steps, and two domains.[20] The first set of samples consisted of GaAs layers of 25, 50, 100, 110, and 500 nm. GaAs layers were deposited at 350 °C (thermocouple), except for the 500 nm sample, with a Ga growth rate of 0.6 MLs^{-1}. A second temperature step at 450 °C (thermocouple) was applied to grow the last 400 nm of the 500 nm thick GaAs sample. A V/III ratio of 2 was maintained for all samples. The low-temperature growth is the key to forming a quasi-two-dimensional nucleation layer of GaAs on Si and the condition for "terrace-driven" initial phase distribution. A second set of 50 nm GaAs samples was grown at thermocouple temperatures ranging from 350 °C to 520 °C, a V/III ratio of 2, and a Ga growth rate of 0.6 MLs^{-1}.

RHEED and AFM were combined to observe the samples' surface morphology. A Brucker AFM dimension 3100 was used to probe the surface of the samples in a classical tapping mode. Each layer was mapped at room temperature for different image sizes (5 × 5, 2 × 2, and 1 × 1 μm^2) with nanosensors probes NCR. TEM was also performed to analyze the structural properties of the APDs. STEM observation lamellas were prepared from the samples using focused ion beam (FIB) ion milling and thinning. Prior to FIB ion milling, the samples were coated with 50 nm of carbon to protect the surface from the platinum mask deposited used for the ion milling process. Ion milling and thinning were carried out in a FEI SCIOS dual-beam FIB–SEM. Initial etching was performed at 30 keV, and final polishing was performed at 5 keV. The lamellas were prepared along the <110> zone axis parallel to the misorientation direction. Finally, samples were observed in an aberration-corrected FEI TITAN 200 TEM-STEM operating at 200 keV. The convergence half-angle of the probe was 17.6 mrad, and the detection inner and outer half-angles for HAADF–STEM were 69 and 200 mrad, respectively. All micrographs were 2048 by 2048 pixels. The dwell time was 8 µs, and the total acquisition time 41 s.

Acknowledgements

A part of this work was supported by the French program on "Investments for the future" (Equipex EXTRA, ANR11-EQPX-0016), the ANR-DFG FILTER project (ANR-20-CE92-0045), the ANR PIANIST (ANR-21-CE09-0020), and NUAGES (ANR-21-CE24-0006) projects, as well as the French Renatech network.

Conflict of Interest

The authors declare no conflict of interest.

Data Availability Statement

The data that support the findings of this study are available from the corresponding author upon reasonable request.

Keywords

III-V on Si, antiphase domains, gallium arsenide, molecular beam epitaxy, semiconductors

Received: December 19, 2022
Revised: April 12, 2023
Published online:

[1] D. Liang, J. E. Bowers, *Nat. Photonics* **2010**, *4*, 511.
[2] Y. Han, H. Park, J. Bowers, K. M. Lau, *Adv. Opt. Photonics* **2022**, *14*, 404.
[3] R. Soref, *Nat. Photonics* **2010**, *4*, 495.
[4] D. Liang, J. E. Bowers, *Light: Adv. Manuf.* **2021**, *2*, 59.
[5] M. Tang, J.-S. Park, Z. Wang, S. Chen, P. Jurczak, A. Seeds, H. Liu, *Prog. Quantum Electron.* **2019**, *66*, 1.
[6] H. Kroemer, *J. Cryst. Growth* **1987**, *81*, 193.
[7] D. J. Chadi, *Phys. Rev. Lett.* **1987**, *59*, 1691.
[8] P. N. Uppal, H. Kroemer, *J. Appl. Phys.* **1985**, *58*, 2195.
[9] M. Akiyama, Y. Kawarada, T. Ueda, S. Nishi, K. Kaminishi, *J. Cryst. Growth* **1986**, *77*, 490.
[10] P. R. Pukite, P. I. Cohen, *Appl. Phys. Lett.* **1987**, *50*, 1739.
[11] A. Georgakilas, J. Stoemenos, K. Tsagaraki, P. Komninou, N. Flevaris, P. Panayotatos, A. Christou, *J. Mater. Res.* **1993**, *8*, 1908.
[12] K. Li, J. Yang, Y. Lu, M. Tang, P. Jurczak, Z. Liu, X. Yu, J. Park, H. Deng, H. Jia, M. Dang, A. M. Sanchez, R. Beanland, W. Li, X. Han, J. Zhang, H. Wang, F. Liu, S. Chen, A. Seeds, P. Smowton, H. Liu, *Adv. Opt. Mater.* **2020**, *8*, 2000970.
[13] J. Yang, K. Li, H. Jia, H. Deng, X. Yu, P. Jurczak, J.-S. Park, S. Pan, W. Li, S. Chen, A. Seeds, M. Tang, H. Liu, *Nanoscale* **2022**, *14*, 17247.
[14] C. Cornet, S. Charbonnier, I. Lucci, L. Chen, A. Létoublon, A. Alvarez, K. Tavernier, T. Rohel, R. Bernard, J.-B. Rodriguez, L. Cerutti, E. Tournié, Y. Léger, M. Bahri, G. Patriarche, L. Largeau, A. Ponchet, P. Turban, N. Bertru, *Phys. Rev. Mater.* **2020**, *4*, 053401.
[15] I. Lucci, S. Charbonnier, L. Pedesseau, M. Vallet, L. Cerutti, J.-B. Rodriguez, E. Tournié, R. Bernard, A. Létoublon, N. Bertru, A. Le Corre, S. Rennesson, F. Semond, G. Patriarche, L. Largeau, P. Turban, A. Ponchet, C. Cornet, *Phys. Rev. Mater.* **2018**, *2*, 060401.
[16] O. Supplie, S. Brückner, O. Romanyuk, H. Döscher, C. Höhn, M. M. May, P. Kleinschmidt, F. Grosse, T. Hannappel, *Phys. Rev. B* **2014**, *90*, 235301.
[17] R. Alcotte, M. Martin, J. Moeyaert, R. Cipro, S. David, F. Bassani, F. Ducroquet, Y. Bogumilowicz, E. Sanchez, Z. Ye, X. Y. Bao, J. B. Pin, T. Baron, *APL Mater.* **2016**, *4*, 046101.
[18] A. Beyer, I. Németh, S. Liebich, J. Ohlmann, W. Stolz, K. Volz, *J. Appl. Phys.* **2011**, *109*, 083529.
[19] A. Beyer, J. Ohlmann, S. Liebich, H. Heim, G. Witte, W. Stolz, K. Volz, *J. Appl. Phys.* **2012**, *111*, 083534.
[20] M. R. Calvo, J.-B. Rodriguez, C. Cornet, L. Cerutti, M. Ramonda, A. Trampert, G. Patriarche, E. Tournié, *Adv. Electron. Mater.* **2022**, *8*, 2100777.
[21] I. Lucci, S. Charbonnier, M. Vallet, P. Turban, Y. Léger, T. Rohel, N. Bertru, A. Létoublon, J.-B. Rodriguez, L. Cerutti, E. Tournié, A. Ponchet, G. Patriarche, L. Pedesseau, C. Cornet, *Adv. Funct. Mater.* **2018**, *28*, 1801585.
[22] H. Takasugi, M. Kawabe, Y. Bando, *Jpn. J. Appl. Phys.* **1987**, *26*, L584.
[23] S. El Kazzi, L. Desplanque, X. Wallart, Y. Wang, P. Ruterana, *J. Appl. Phys.* **2012**, *111*, 123506.
[24] T. Shitara, J. Zhang, J. H. Neave, B. A. Joyce, *J. Cryst. Growth* **1993**, *127*, 494.
[25] K. Ohta, T. Kojima, T. Nakagawa, *J. Cryst. Growth* **1989**, *95*, 71.